PAPER

A low-T_c superconducting modification of Th$_4$H$_{15}$ synthesized under high pressure

IOP ebooks™

Bringing together innovative digital publishing with leading authors from the global scientific community.

Start exploring the collection−download the first chapter of every title for free.

A low-T_c superconducting modification of Th$_4$H$_{15}$ synthesized under high pressure

N N Wang[1,2], **P F Shan**[1,2], **K Y Chen**[1,2], **J P Sun**[1,2], **P T Yang**[1,2], **X L Ma**[1], **B S Wang**[1,2,3],
X H Yu[1,2,3], **S Zhang**[1,2], **G F Chen**[1,2,3], **J-G Cheng**[1,2] (iD), **X L Dong**[1,2,3] (iD), **X H Chen**[4,5] (iD)
and Z X Zhao[1,2,3]

[1] Beijing National Laboratory for Condensed Matter Physics and Institute of Physics, Chinese Academy of Sciences, Beijing 100190, People's Republic of China
[2] School of Physical Sciences, University of Chinese Academy of Sciences, Beijing 100190, People's Republic of China
[3] Songshan Lake Materials Laboratory, Dongguan, Guangdong 523808, People's Republic of China
[4] Hefei National Laboratory for Physical Sciences at Microscale and Department of Physics, University of Science and Technology of China, Hefei, Anhui 230026, People's Republic of China
[5] Key Laboratory of Strongly-coupled Quantum Matter Physics, Chinese Academy of Sciences, University of Science and Technology of China, Hefei, Anhui 230026, People's Republic of China

E-mail: jgcheng@iphy.ac.cn

CrossMark

Abstract

Among the metal hydrides, Th$_4$H$_{15}$ is the first reported superconductor with a relatively high $T_c \approx 8$ K at ambient pressure. Here we report on the synthesis and characterization of a low-T_c superconducting modification of Th$_4$H$_{15}$, which is obtained via hydrogenating Th metal at 5 GPa and 800 °C by using the ammonia borane as the hydrogen source. Measurements of resistivity, magnetic susceptibility, and specific heat confirm that the obtained Th$_4$H$_{15}$ sample shows a bulk superconducting transition at $T_c \approx 6$ K, which is about 2 K lower than that reported previously. Various characteristic superconducting parameters have been extracted for this compound and unusual lattice dynamics were evidenced from the specific-heat analysis.

Keywords: Th$_4$H$_{15}$, metal hydrides, superconductivity, high pressure

(Some figures may appear in colour only in the online journal)

1. Introduction

Recently, the hydrogen-rich compounds have attracted considerable research interest because they hold the promise to achieve room-temperature superconductivity (SC) [1–13]. One important breakthrough is the recent observation of SC in the super-hydride LaH$_{10 \pm \delta}$ with T_c up to 250–260 K under ultra-high pressures of 170–200 GPa [10, 11]. So far, many binary metal hydrides have been theoretically investigated and some of them are experimentally confirmed to be high-T_c superconductors under high pressures [2–11, 14–17]. In a recent work by Semenok *et al*, several metastable phases of ThH$_X$ with different H contents, e.g. ThH$_4$, ThH$_6$, ThH$_9$,

ThH$_{10}$, were synthesized under high pressures and the latter two compounds were found to be superconductors with high $T_c \approx 146$ K and 160 K, respectively [14, 18]. Because these hydrogen-rich materials can only be stabilized under ultrahigh pressure conditions [18], detailed characterizations on their superconducting properties that are essential for understanding the superconducting mechanisms are hampered to a large extent. A recent theoretical calculation argued that the Th super-hydrides should be classified to unconventional superconductors [19].

Actually, the low-H compound Th$_4$H$_{15}$ (or ThH$_{3.75}$) is the first-known superconductor among the metal hydrides, and it has been subjected to many studies in 1970s [20–30].

Different from the above-mentioned metastable ThH_x, Th_4H_{15} synthesized by reacting the Th metal with hydrogen in a sealed condition is stable at ambient conditions. In this regard, Th_4H_{15} can be taken as a proxy to investigate the mechanism of SC, even though it has a relatively low T_c compared with the superhydrides mentioned above. Previous studies have provided some information about the normal and superconducting states of Th_4H_{15} based on the electrical transport [20, 21, 26], magnetic susceptibility [20, 21], nuclear magnetic resonance (NMR) [29, 30], thermodynamic measurements [23, 24] and theoretical calculations [19, 27, 31, 32], but no consensus has been reached about the superconducting mechanism. According to Satterthwaite *et al*, the coupling between electrons and hydrogen vibration modes may enhance the superconducting interactions [20, 21], and the NMR experiments suggest that the electrons of hydrogen contribute to the conduction band of Th_4H_{15} [30]. The absence of obvious isotope effect in Th_4H_{15}–Th_4D_{15} questions the electron–phonon mechanism [26]. In addition, the heat capacity data indicate that the electron–phonon coupling cannot give such a high T_c in Th_4H_{15} [23, 24], but the high frequency hydrogen-atom vibration may contribute to the high T_c [28]. To explain the positive pressure effect on the superconducting T_c, Dietrich *et al* proposed that the 5*f* bands of Th intersect the Fermi level [22]. Therefore, the nature of SC in Th_4H_{15} is still under debate and requires more investigations.

These above-mentioned discrepancies should be largely attributed to the variations of studied samples. In the previous studies, bulk polycrystalline Th_4H_{15} samples were usually prepared under a moderate hydrogen pressure, i.e. 600–800 atm [21, 26], and the superconducting T_c was found to vary in the range between 7.5 and 8.5 K depending the actual hydrogen concentration while the x-ray diffraction (XRD) shows no difference [21]. It was confirmed that both the 'Th_4H_{15}' type structure and the SC can be retained for the H/Th ratio decreasing from 3.75 to 3.25 [26]. Interestingly, previous studies have identified two kinds of superconducting modifications of Th_4H_{15} showing a higher $T_c \approx 9$ K and a lower $T_c \approx 8$ K, respectively, but they are found to possess stoichiometric composition and identical lattice parameters [22]. A third non-superconducting modification with a tetragonal distortion was also observed upon water uptaken in Th_4H_{15} [26].

In this work, we have adopted a different procedure to synthesize bulk polycrystalline Th_4H_{15} samples by hydrogenating Th metal under high-pressure and high-temperature conditions in a Kawai-type multianvil module. We find that the as-obtained Th_4H_{15} has a superconducting $T_c \approx 6$ K, which is about 2 K lower than that reported previously. The physical properties of this new low-T_c modification of Th_4H_{15} have been studied in detail based on the measurements of resistivity, magnetic susceptibility and specific heat as well as pressure effects. Characteristic parameters associated with the normal and superconducting states of Th_4H_{15} were extracted. Our results indicate that Th_4H_{15} is a type-II superconductor with unusual lattice dynamics.

2. Experimental details

Polycrystalline Th_4H_{15} samples were synthesized by hydrogenating Th metal under high-pressure and high-temperature conditions in a Kawai-type multianvil module (Max Voggenreiter GmbH). The ammonia borane (BH_3NH_3) was employed as the hydrogen-releasing agent in the sealed high-pressure chamber [18, 33–35]. The Th metal sandwiched in between two BH_3NH_3 pellets was contained in a sealed gold capsule, which is placed in a cylindrical graphite heater and then subjected to heat treatment at 800°C for 60 min under 5 GPa. To maintain a sufficient hydrogen gas, we have used the molar ratio of BH_3NH_3/Th to be greater than 2. The temperature was quenched to room temperature before releasing pressure slowly, and then the sample was recovered at ambient condition.

The resultant pellets are black with metallic luster, and the phase purity was checked by using XRD at room temperature. The structural parameters were extracted via refining the XRD pattern with the Fullprof program. It should be noted that the obtained Th_4H_{15} polycrystalline sample is stable in a dry condition for quite a long period, but it degrades gradually in the presence of moisture at ambient pressure. We confirm that the XRD pattern remains unchanged after being stored in the desiccator for several days, but a large amount of ThO_2 appears in the XRD pattern when exposing the sample in the humid air. Therefore, we stored the Th_4H_{15} samples in the Ar-filled glove box with controlled oxygen and water content. In the present study, our samples' synthesis method does not allow a direct determination of the H content as done in the previous studies [20, 26], in which the H content was determined by monitoring the volume change of the hydrogen gas before and after the reaction between Th and hydrogen in a sealed tube. In addition, the commonly used methods for chemical element analysis such as the energy-dispersive spectroscopy are also infeasible due to the light-mass nature of hydrogen. We thus did not determine the exact H content for our samples in the present study.

The temperature dependences of resistivity and heat capacity were measured with a physical property measurement system, while the magnetic properties were measured with a magnetic property measurement system from Quantum Design. The effect of pressure on the electrical transport properties was investigated by measuring resistivity with the standard four-probe method under various hydrostatic pressures up to 8 GPa with a palm cubic anvil cell apparatus [36, 37]. The pressure values were determined according to the pressure-loading force calibration curve, which was established by observing the phase transitions of Bi (2.55, 2.7, 7.7 GPa) and Pb (13.4 GPa) at room temperature [36]. We employed glycerol as the pressure transmitting medium in our study because glycerol has a relatively high solidification pressure of $\sim$6 GPa at room temperature [38]. The sample dimensions for the high-pressure resistivity measurements are $0.31 \times 0.12 \times 0.65$ mm^3.
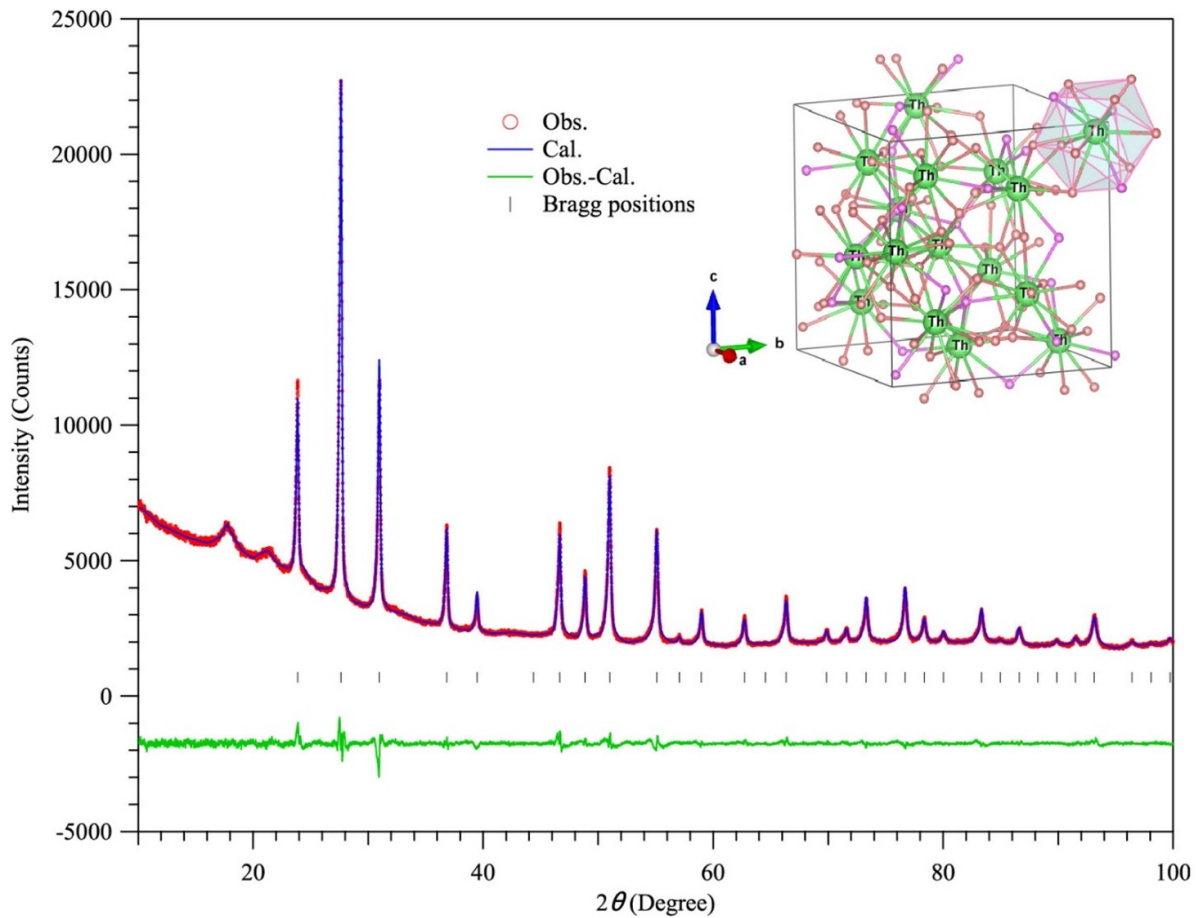
Figure 1. Observed, calculated and difference XRD profiles of Th_4H_{15} measured at room temperature after Rietveld refinements. The Bragg positions are shown as the tick marks. The inset shows the crystal structure of Th_4H_{15}.

Table 1. The mass (molar) ratio of BH_3NH_3/Th for different samples during synthesis experiments. Lattice parameter and T_c (T_c^{mid}) of different samples are also listed.

Sample label	Mass ratio BH_3NH_3/Th	Molar ratio released hydrogen/Th	Lattice parameter a (Å)	(T_c^{mid}) (K)
S1	0.28	8.40	9.1237(1)	5.5
S2	0.34	10.24	9.1242(2)	5.3
S3	0.42	12.64	9.1277(1)	4.7

3. Results and discussion

Figure 1 shows a representative XRD pattern of Th_4H_{15} collected at room-temperature, and it confirms that we have obtained a single-phase sample. The XRD data can be refined with the body centered cubic structure (space group: *I-43d*, No. 220) by using the Rietveld method in FullProf program. As illustrated in figure 1, the refinements are well converged with reliable factors $R_p = 1.87\%$, $R_{exp} = 1.94\%$ and $\chi^2 = 1.71$. The obtained lattice parameters are listed in table 1. Although all the values are in good agreement with those reported previously [26, 39], we found that the lattice parameter increases slightly with increasing the initial BH_3NH_3/Th ratio. This observation indicates that the H-concentration in Th_4H_{15} might be varied by adjusting the available hydrogen

source. Displayed in the inset of figure 1 is the crystal structure of Th_4H_{15}, which consists of 16 equivalent Th atoms and 60 H atoms in the unit cell. The Th atoms form a network of corner-sharing tetrahedra with the tetrahedral edge length ranging from 3.87 to 4.10 Å. Th atom is coordinated by three H_I and nine H_{II} atoms, forming a cage structure with interatomic distances of $Th–H_I = 2.46$ Å and $Th–H_{II} = 2.29$ Å [39], respectively. The H_I atoms are located at the centers of the Th tetrahedra and H_{II} atoms at the centers of triangles formed by Th atoms.

Figure 2(a) shows the low-temperature magnetization $M(T)$ of Th_4H_{15} measured at a magnetic field of 5 Oe under zero-field-cooled (ZFC) and field-cooled (FC) conditions. An obvious diamagnetic signal is observed in the ZFC curve, corresponding to the appearance of superconducting transition
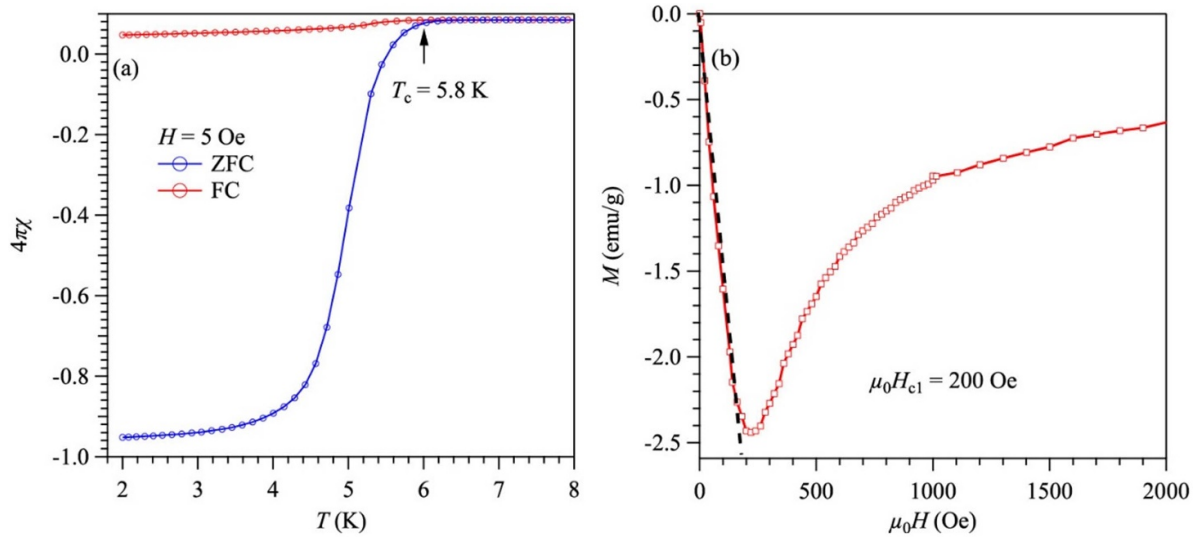
Figure 2. (a) Temperature dependence of the magnetization $M(T)$ of Th_4H_{15} in an applied magnetic field of $H = 5$ Oe. (b) The isothermal magnetization M versus H curve at $T = 2$ K.
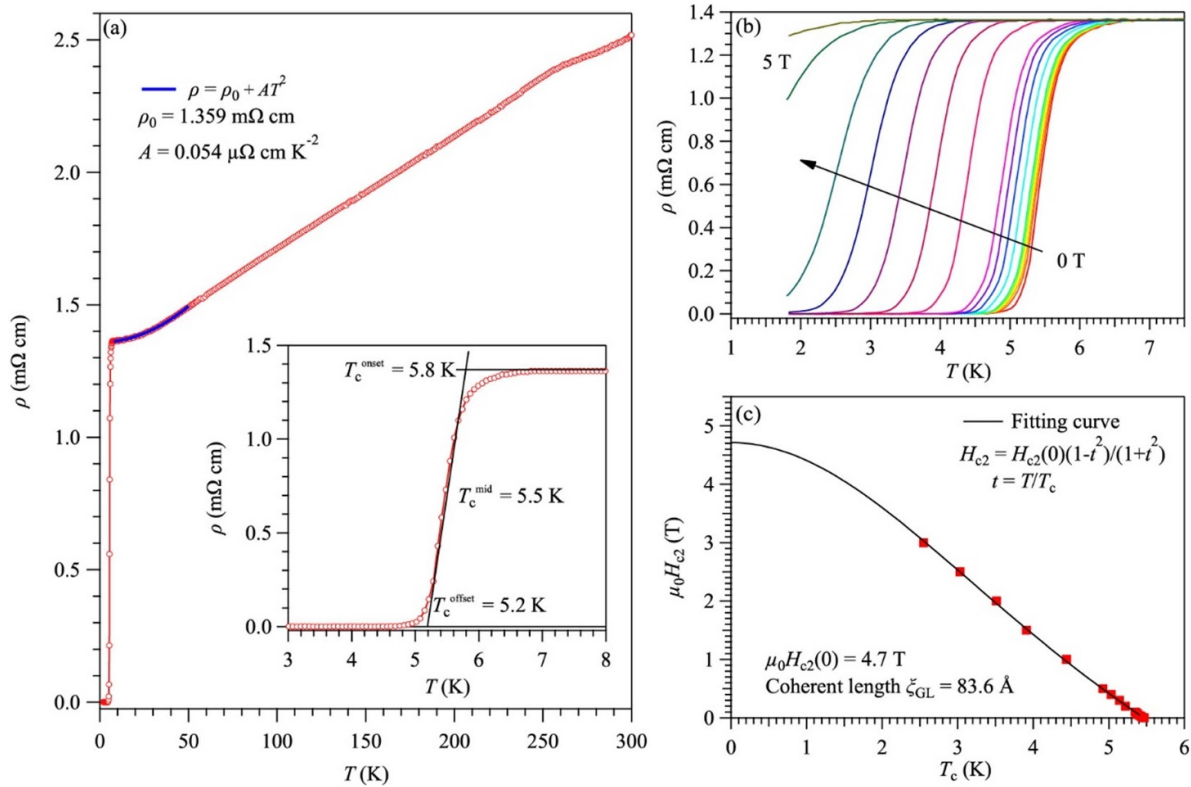

Figure 3. (a) Temperature dependence of the resistivity $\rho(T)$ of Th_4H_{15} at zero magnetic field. The inset shows low-temperature part around T_c. (b) The superconducting transition in resistivity under various magnetic fields. (c) Temperature dependence of the upper critical field H_{c2} for Th_4H_{15}. The solid line is the fitting curve by using the formula $H_{c2} = H_{c2}(0)(1-t^2)/(1+t^2)$, where $t = T/T_c$.

at $T_c \approx 5.8$ K, which is about 2 K lower than that of 7.5–8.5 K reported previously [21]. As mentioned above, the T_c of Th_4H_{15} can vary in the range 7–8 K depending on the H-concentration, no samples were found to exhibit a T_c lower than 6 K as observed here. The much reduced $M(T)$ under FC process indicates a weak pinning effect as the evidence for type-II superconductor. Figure 2(b) presents the field dependence of magnetization $M(H)$ up to 2000 Oe at 2 K. Apparently, the large magnetic hysteresis characterizes the common behavior of type-II superconductors. A linear fitting to $M(H)$ for the full shielding effect yields the lower critical field, $\mu_0H_{c1}(2\ K) = 200$ Oe [40, 41].
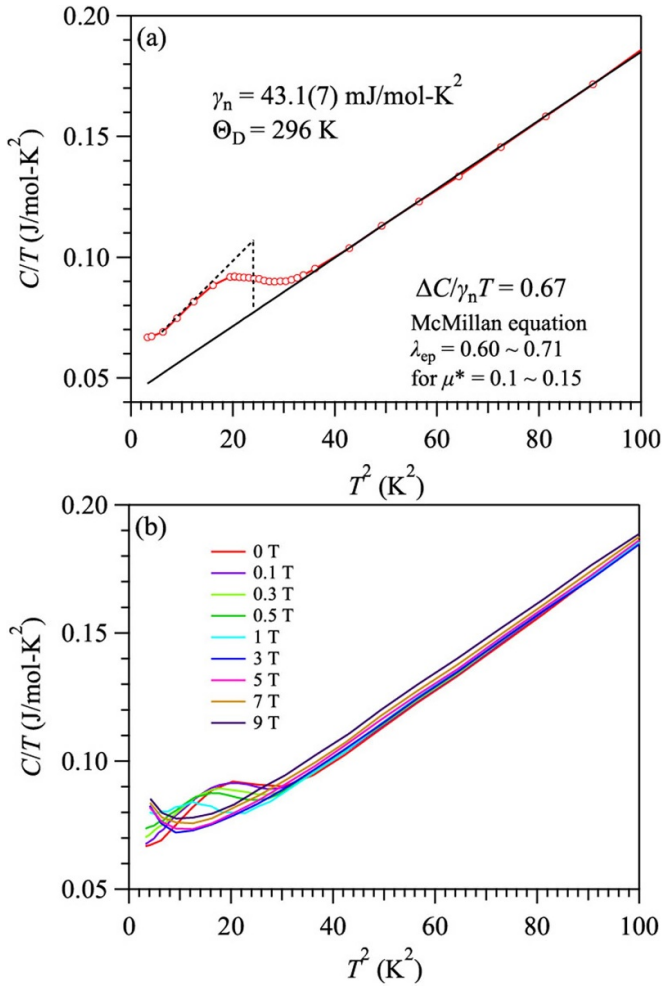
Figure 4. (a) Specific heat divided by temperature (*C/T*) versus T^2 measured at 0 T. The black solid line is the normal-state fitting curve. The black dotted line shows the specific heat jump near T_c, and $\Delta C/\gamma_n T$ is estimated by entropy conservation near T_c. (b) Specific heat divided by temperature *C/T* versus T^2 under various magnetic fields.

The sample's synthesis method and reaction condition in this work are different from the previous ones. The bulk polycrystalline Th_4H_{15} sample in the previous studies was obtained via hydrogenation of the Th metal under a moderate hydrogen-gas pressure, i.e. 600–800 atm, while it was prepared at much higher pressure, i.e. 5 GPa and 800 °C, in the present study by employing solid BH_3NH_3 as the hydrogen releasing agent in the sealed chamber. In addition, we have used extra BH_3NH_3 to maintain a sufficient hydrogen source. As such, we suspect that more hydrogen might enter the crystal lattice under high pressure, forming the H_2-like molecules and embedded around the hydrogen cage. This might cause the local lattice distortion and the reduction of the electronic density of states at Fermi level, thus resulting in a lower T_c as observed. Such a scenario is consistent with the fact that T_c decreases gradually with increasing the initial ratio of BH_3NH_3/Th as shown in table 1.

To characterize the electrical transport properties of Th_4H_{15} at the normal and superconducting states, we measured the temperature and field dependences of resistivity $\rho(T)$ as shown

in figures 3(a) and (b). The normal-state $\rho(T)$ exhibits a typical metallic behavior with the residual resistivity ratio RRR $= \rho(300\ \text{K})/\rho(7\ \text{K}) = 1.85$ and the Fermi-liquid behavior at low temperatures. As shown by the solid line in figure 3(a), the $\rho(T)$ at $T < 50$ K in the normal state can be fitted excellently by the expression $\rho = \rho_0 + AT^2$, where ρ_0 is the residual resistivity due to the defects and/or impurities scattering, and the temperature coefficient A is proportional to the effective mass of charge carriers induced by electron–electron scattering processes [42]. The best fit yields $\rho_0 = 1.36\ \text{m}\Omega\ \text{cm}$ and $A = 0.054\ \mu\Omega\ \text{cm}\ \text{K}^{-2}$. An enlarged view of the superconducting transition is depicted in the inset of figure 3(a), which shows that $\rho(T)$ starts to drop around 6 K and reaches zero resistance at ~5 K. Here, the $T_c^{\text{onset}} \approx 5.8$ K and $T_c^{\text{offset}} \approx 5.2$ K are determined as the interceptions between two straight lines below and above the superconducting transitions. These values are consistent with that determined from the $M(T)$ data shown above.

Under magnetic fields, the superconducting transition of Th_4H_{15} is continuously shifted to lower temperatures and becomes broadened up gradually as shown in figure 3(b). The T_c is suppressed to below 2 K at 5 T. Here, we have determined the T_c^{mid} from the $\rho(T)$ curves and plotted the temperature dependence of the upper critical field $\mu_0 H_{c2}(T)$ in figure 3(c). As can be seen, the $\mu_0 H_{c2}(T)$ can be well fitted by using the empirical formula: $H_{c2}(T) = H_{c2}(0)(1-t^2)/(1 + t^2)$, where $t = T/T_c$ [43–45]. The obtained upper critical field $\mu_0 H_{c2}(0) = 4.7$ T can be used to estimate the Ginzburg–Landau (G–L) coherent length $\xi_{\text{GL}} = 83.6$ Å based on the formula: $\mu_0 H_{c2} = \Phi_0/2\pi\xi_{\text{GL}}^2$, where $\Phi_0 = hc/2e$ is the magnetic flux quantum. Furthermore, according to the relationship that $H_{c1} = (\Phi_0/4\pi\lambda_{\text{GL}}^2)\ln(\lambda_{\text{GL}}/\xi_{\text{GL}})$, we can further estimate the penetration depth $\lambda_{\text{GL}} = 84.3$ Å [46]. Then, the calculated G–L parameter $\kappa_{\text{GL}} = \lambda_{\text{GL}}/\xi_{\text{GL}} = 1.01$ that is larger than $1/\sqrt{2}$ further confirms that Th_4H_{15} belongs to the type-II superconductor [41, 47].

To further characterize the superconducting properties of Th_4H_{15}, we also measured its low-temperature specific heat $C(T)$, which displays an obvious jump at $T_c \approx 5.7$ K, confirming the bulk nature of the superconducting transition. The observed T_c is in excellent agreement with the magnetization and resistivity measurements. It is noted that the observed $C(T)$ anomaly at T_c is not very sharp, presumably due to the polycrystalline nature of the studied sample. At the normal state, the $C(T)$ follows a straight line in the plot of C/T vs T^2, figure 4(a), and a linear fitting to $C_n(T) = \gamma_n T + \beta T^3$ yields the Sommerfeld coefficient $\gamma_n = 43.1(7)$ mJ mol^{-1} K^{-2} and $\beta = 1.42(1)$ mJ mol^{-1} K^{-4}. The large γ_n value implies a relatively large effective electron mass and thus enhanced electron correlations. The Debye temperature $\Theta_D \approx 296$ K can be calculated according to the relation $\Theta_D = (12\pi^4 nR/5\beta)^{1/3}$, where $R = 8.314$ J mol^{-1} K^{-1} is the ideal gas constant, and $n = 19$ is the number of atoms per formula unit. The specific heat jump at T_c gives $\Delta C/\gamma_n T \approx 0.67$, which is much smaller than the weak-coupling BCS limit ~1.43 for the *s*-wave superconductors. Such a large discrepancy should be attributed to the rather diminished specific-heat anomaly at T_c as mentioned above. Based on the obtained Θ_D, we
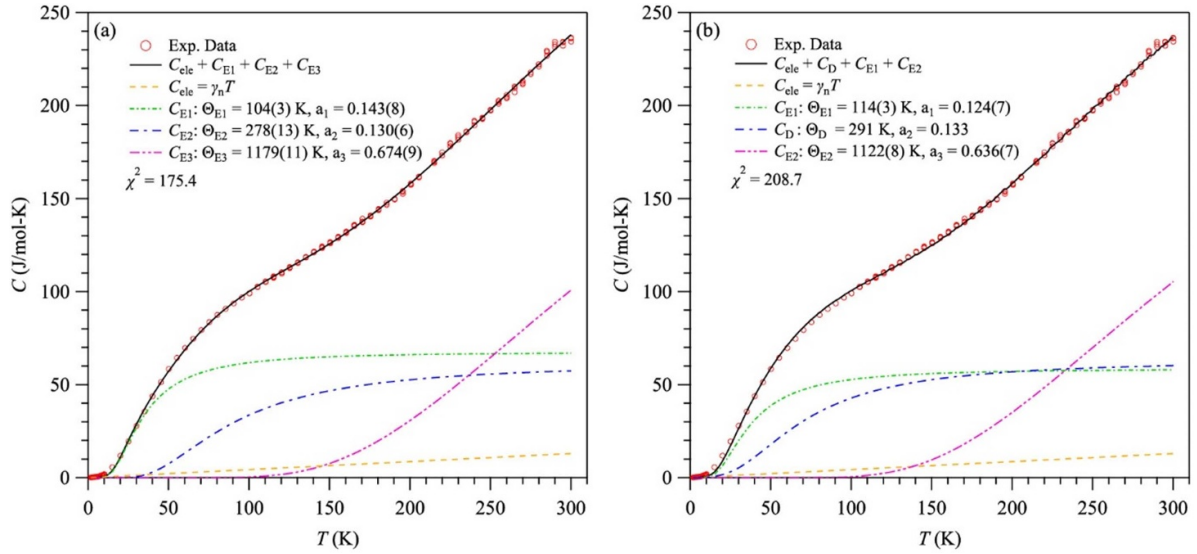
Figure 5. Temperature-dependent specific heat $C(T)$ of Th_4H_{15} in the whole temperature range at zero magnetic field. The data are analyzed with two models as explained in the main text.

can also calculate the dimensionless electron–phonon coupling constant λ_{ep} by using the McMillan formula: $\lambda_{ep} = \frac{1.04 + \mu^* \ln\left(\frac{\Theta_D}{1.45 T_c}\right)}{(1 - 0.62\mu^*) \ln\left(\frac{\Theta_D}{1.45 T_c}\right) - 1.04}$, where μ^* is the material specific Coulomb pseudopotential [47, 48]. By employing $\mu^* = 0.1 \sim 0.15$, we obtained a $\lambda_{ep} = 0.6 \sim 0.7$, which is comparable to the medium coupling strength $\lambda_{ep} = 0.68$ [41]. Figure 4(b) shows the C/T versus T^2 under various magnetic fields. With increasing the magnetic field, the C/T anomaly at T_c is suppressed gradually as expected. However, C/T shows an anomalous upturn at low temperatures for $H \geqslant 3$ T, which might be attributed to the nuclear Schottky contribution [49].

To gain more insight on the physical properties of Th_4H_{15}, we also measured its $C(T)$ in the whole temperature range from 300 K to low temperatures. As shown in figure 5, the $C(T)$ of Th_4H_{15} exhibits a broad hump centered around 70 K followed by a nearly linear increase above 200 K upon warming up. In addition, the specific heat at room-temperature, $\sim$240 J mol^{-1} K^{-1}, is far below the predicted value of the Dulong-Petit law, i.e. $3nR = 474$ J mol^{-1} K^{-1}. These observations imply the presence of unusual lattice dynamics in Th_4H_{15}. To account for the measured $C(T)$, here we have simulated the lattice specific heat, C_{lat}, by considering the Einstein and/or Debye models [50], *viz.*

$$C(T) = \gamma_n T + 3nR \sum_{i=1}^{3} a_i \left(\frac{\Theta_{Ei}}{T}\right)^2 \frac{\exp(\Theta_{Ei}/T)}{\left[\exp\left(\frac{\Theta_{Ei}}{T}\right) - 1\right]^2} \quad (1)$$

$$C(T) = \gamma_n T + 3nR \sum_{i=1}^{2} a_i \left(\frac{\Theta_{Ei}}{T}\right)^2 \frac{\exp(\Theta_{Ei}/T)}{\left[\exp\left(\frac{\Theta_{Ei}}{T}\right) - 1\right]^2} + 9nR a_3 \left(\frac{T}{\Theta_D}\right)^3 \int_0^{\Theta_D/T} \frac{e^x x^4}{(e^x - 1)^2}. \quad (2)$$

The first equation describes C_{lat} by using three Einstein terms, while the second one using two Einstein term plus one Debye term [50]. As shown in figures 5(a) and (b), both equations can fit the $C(T)$ excellently in the whole temperature range, and similar fitting results are obtained as illustrated by the separate contribution from each term. In addition to two low-frequency phonons, we observe a large portion of contribution from a high-frequency phonon with an Einstein temperature $\sim$1100 K, which accounts for the almost linear increase of $C(T)$ above 200 K. Such a high frequency of phonon should be attributed to the optical phonons associated with the light-mass hydrogen lattice, which may be also responsible for the observed SC in Th_4H_{15}.

The presence of high-frequency phonon associated with hydrogen lattice would predict an obvious isotope effect, which, if confirmed by further experiments, will contradict with the previous studies [20, 26] that show the absence of or a small reverse isotope effect and then imply a drastic difference between our sample with a lower T_c and those reported previously. On the other hand, if the negative isotope effect is observed as seen in the PdH_x–PdD_x–PdT_x system, large zero point effects [51, 52], electron–electron interaction [53], anharmonicity and other quantum nuclear effects [54, 55] have to be taken into consideration.

Finally, the effect of pressure on the T_c of Th_4H_{15} is investigated by measuring its $\rho(T)$ up to 8 GPa in a cubic-anvil-cell apparatus. As shown in figure 6(a), the magnitude of $\rho(T)$ in the normal state first decreases significantly up to 3 GPa, then shows an anomalous increase at 5 GPa, and then decreases again at 8 GPa. But the behaviors of $\rho(T)$ for all pressure are almost identical. An enlarged view of the low-temperature $\rho(T)$ below 10 K is displayed in the inset of figure 6(a), which shows a nonmonotonic variation of the superconducting transition as a function of pressure. It should be noted that the superconducting transition in resistivity becomes relatively broad at high pressures, which makes the assessments of T_c and its
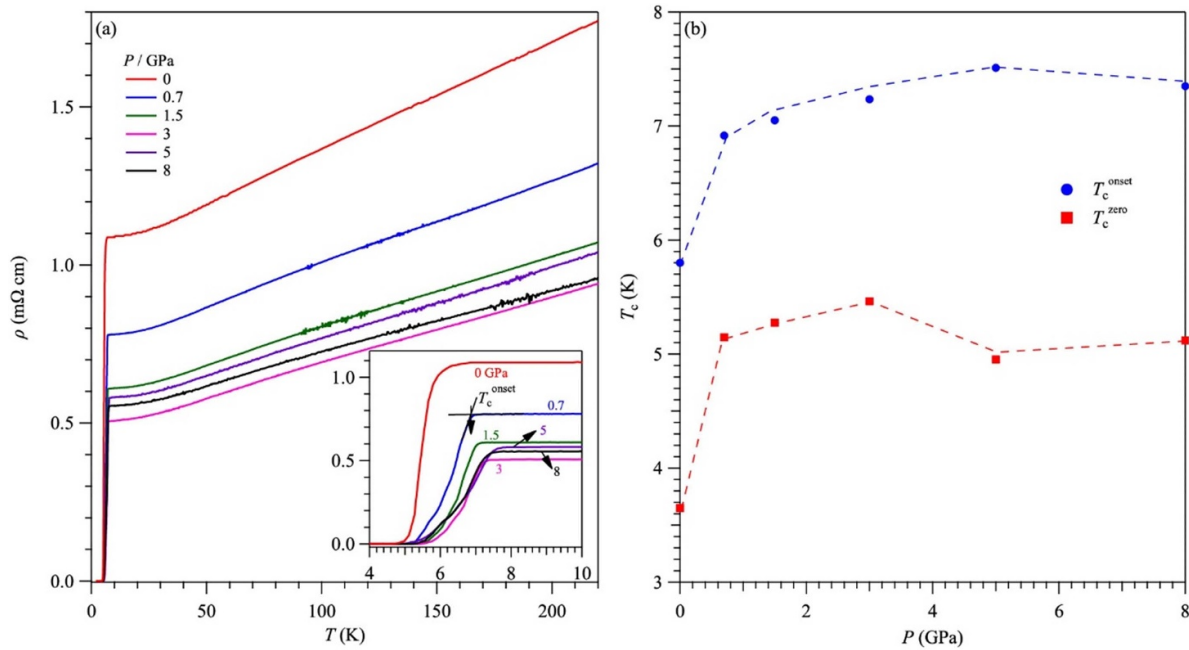
Figure 6. (a) Temperature dependence of resistivity $\rho(T)$ of Th_4H_{15} under various hydrostatic pressures up to 8 GPa. The inset shows the low temperature range around the superconducting transition. (b) Temperature-pressure phase diagram of Th_4H_{15}. The error bar of T_c is less than the symbol.

variation with pressure less accurate. Here, we determine the T_c^{onset} by using the intersection between two straight lines below and above the superconducting transitions and T_c^{zero} as the temperature for zero resistance. The pressure dependences of T_c^{onset} and T_c^{zero} for Th_4H_{15} are shown in figure 6(b). As can be seen, the T_c^{onset} is first enhanced quickly from 5.8 K at ambient pressure to 6.9 K at 0.7 GPa and then increases gradually to $\sim$7.5 K at 5 GPa before decreasing slightly to $\sim$7.2 K at 8 GPa. A positive pressure dependence of $T_c(P)$ for Th_4H_{15} has also been reported by Dietrich *et.al* [22], but the highest pressure in the previous study was 2.8 GPa. Here, our measurements in a larger pressure range enable us to evidence an initial positive pressure coefficient and then a relatively stable or slight downward trend above 5 GPa. For a conventional BCS superconductor, such a non-monotonic $T_c(P)$ implies that two competing factors should be at play under pressure. For example, pressure might enhance the density of state at Fermi energy, leading to an increase of T_c, while the lattice hardening under pressure would reduce T_c. Further theoretical studies on the electronic and phonon properties as a function of pressure are needed in order to understand the above experimental observations.

4. Conclusion

In summary, we have synthesized the polycrystalline Th_4H_{15} sample under high pressure conditions and characterized its structural, magnetic, electrical transport and thermodynamics properties in detail. It is confirmed that our sample is a low-T_c superconducting modification compared to the previous reports, and the T_c is found to be sensitive to the H content. Our work reveals that Th_4H_{15} is a type-II superconductor with moderate electron–phonon coupling. The analysis of the lattice specific heat evidenced the presence of high-frequency optical phonons which might be responsible for the observed SC in Th_4H_{15} with a relatively high T_c.

ORCID iDs

J-G Cheng ⬤ https://orcid.org/0000-0002-4969-1960
X L Dong ⬤ https://orcid.org/0000-0002-6268-2049
X H Chen ⬤ https://orcid.org/0000-0001-6947-1407

References

[1] Ashcroft N W 2004 *Phys. Rev. Lett.* **92** 187002
[2] Duan D, Liu Y, Tian F, Li D, Huang X, Zhao Z, Yu H, Liu B, Tian W and Cui T 2014 *Sci. Rep.* **4** 6968
[3] Drozdov A P, Eremets M I, Troyan I A, Ksenofontov V and Shylin S I 2015 *Nature* **525** 73

[4] Einaga M, Sakata M, Ishikawa T, Shimizu K, Eremets M I, Drozdov A P, Troyan I A, Hirao N and Ohishi Y 2016 *Nat. Phys.* **12** 835

[5] Peng F, Sun Y, Pickard C J, Needs R J, Wu Q and Ma Y M 2017 *Phys. Rev. Lett.* **119** 107001

[6] Geballe Z M, Liu H, Mishra A K, Ahart M, Somayazulu M, Meng Y, Baldini M and Hemley R J 2018 *Angew. Chem., Int. Ed. Engl.* **57** 688

[7] Liu H Y, Naumov I I, Geballe Z M, Somayazulu M, Tse J S and Hemley R J 2018 *Phys. Rev. B* **98** 100102

[8] Boeri L and Bachelet G B 2019 *J. Phys.: Condens. Matter.* **31** 234002

[9] Heil C, Di Cataldo S, Bachelet G B and Boeri L 2019 *Phys. Rev. B* **99** 220502

[10] Drozdov A P *et al* 2019 *Nature* **569** 528

[11] Somayazulu M, Ahart M, Mishra A K, Geballe Z M, Baldini M, Meng Y, Struzhkin V V and Hemley R J 2019 *Phys. Rev. Lett.* **122** 027001

[12] Sun Y, Lv J, Xie Y, Liu H Y and Ma Y M 2019 *Phys. Rev. Lett.* **123** 097001

[13] Snider E, Dasenbrock-Gammon N, McBride R, Debessai M, Vindana H, Vencatasamy K, Lawler K V, Salamat A and Dias R P 2020 *Nature* **586** 373

[14] Kvashnin A G, Semenok D V, Kruglov I A, Wrona I A and Oganov A R 2017 *ACS Appl. Mater. Interfaces* **10** 43809

[15] Liu H Y, Naumov I I, Hoffmann R, Ashcroft N W and Hemley R J 2017 *Proc. Natl Acad. Sci. USA* **114** 6990

[16] Salke N P *et al* 2019 *Nat. Commun.* **10** 4453

[17] Zhou D, Semenok D V, Duan D, Xie H, Chen W, Huang X, Li X, Liu B, Oganov A R and Cui T 2020 *Sci. Adv.* **6** eaax6849

[18] Semenok D V, Kvashnin A G, Ivanova A G, Svitlyk V, Fominski V Y, Sadakov A V, Sobolevskiy O A, Pudalov V M, Troyan I A and Oganov A R 2020 *Mater. Today* **33** 36

[19] Talantsev E F and Mataira R C 2020 *Mater. Res. Express* **7** 016003

[20] Satterthwaite C B and Toepke I L 1970 *Phys. Rev. Lett.* **25** 741

[21] Satterthwaite C B and Peterson D T 1971 *J. Less-Common Met.* **26** 361

[22] Dietrich M, Gey W, Rietschel H and Satterthwaite C B 1974 *Solid State Commun.* **15** 941

[23] Schmidt H G and Wolf G 1975 *Solid State Commun.* **16** 1085

[24] Miller J F, Caton R H and Satterthwaite C B 1976 *Phys. Rev. B* **14** 2795

[25] Winter H and Ries G 1976 *Z. Phys. B* **24** 279

[26] Caton R and Satterthwaite C B 1977 *J. Less-Common Met.* **52** 307

[27] Weaver J H, Knapp J A, Eastman D E, Peterson D T and Satterthwaite C B 1977 *Phys. Rev. Lett.* **39** 639

[28] Dietrich M, Reichardt W and Rietschel H 1977 *Solid State Commun.* **21** 603

[29] Lau K F, Vaughan R W and Satterthwaite C B 1977 *Phys. Rev. B* **15** 2449

[30] Peretz M, Zamir D and Hadari Z 1978 *Phys. Rev. B* **18** 2059

[31] Shein I R, Shein K I, Medvedeva N I and Ivanovskii A L 2007 *Physica B* **389** 296

[32] Wang B T, Zhang P, Song H Z, Shi H L, Li D F and Li W D 2010 *J. Nucl. Mater.* **401** 124

[33] Wolf G, Baumann J, Baitalow F and Hoffmann F P 2000 *Thermochim. Acta* **343** 19

[34] Baitalow F, Baumann J, Wolf G, Jaenicke-Rößler K and Leitner G 2002 *Thermochim. Acta* **391** 159

[35] Frueh S, Kellett R, Mallery C, Molter T, Willis W S, King'ondu C and Suib S L 2011 *Inorg. Chem.* **50** 783

[36] Cheng J G, Matsubayashi K, Nagasaki S, Hisada A, Hirayama T, Hedo M, Kagi H and Uwatoko Y 2014 *Rev. Sci. Instrum.* **85** 093907

[37] Cheng J G, Wang B S, Sun J P and Uwatoko Y 2018 *Chin. Phys. B* **27** 077403

[38] Klotz S, Takemura K, Strässle T and Hansen T 2012 *J. Phys.: Condens. Matter.* **24** 325103

[39] Zachariasen W H 1953 *Acta Cryst.* **6** 393

[40] Abdel-Hafiez M *et al* 2018 *Phys. Rev. B* **97** 134508

[41] Górnicka K, Das D, Gutowska S, Wiendlocha B, Winiarski M J, Klimczuk T and Kaczorowski D 2019 *Phys. Rev. B* **100** 214514

[42] Mott N F 1972 *Phil. Mag. J. Theor. Exp. Appl. Phys.* **26** 1249

[43] Helfand E and Werthamer N R 1966 *Phys. Rev.* **147** 288

[44] Werthamer N R, Helfand E and Hohenberg P C 1966 *Phys. Rev.* **147** 295

[45] Kase N, Kittaka S, Sakakibara T and Akimitsu J 2012 *J. Phys. Soc. Japan* **81** SB016

[46] Brandt E H 2003 *Phys. Rev. B* **68** 054506

[47] Xu Y, Jöhr S, Das L, Kitagawa J, Medarde M, Shiroka T, Chang J and Shang T 2020 *Phys. Rev. B* **101** 134513

[48] McMillan W L 1968 *Phys. Rev.* **167** 331

[49] Wang W D *et al* 2012 *J. Low Temp. Phys.* **171** 127

[50] Yu W C, Cheung Y W, Saines P J, Imai M, Matsumoto T, Michioka C, Yoshimura K and Goh S K 2015 *Phys. Rev. Lett.* **115** 207003

[51] Ke X Z and Kramer G J K 2002 *Phys. Rev. B* **66** 553

[52] Ostanin S, Borisov V, Fedorov D, Salamatov E and Mertig I 2019 *J. Phys.: Condens. Matter.* **31** 075703

[53] Villa-Cortés S and Baquero R 2018 *J. Phys. Chem. Solids* **119** 80

[54] Errea I, Calandra M and Mauri F 2013 *Phys. Rev. Lett.* **111** 177002

[55] Errea I, Calandra M and Mauri F 2014 *Phys. Rev. B* **89** 064302